

# Probabilistic delamination diagnosis of composite materials using a novel Bayesian Imaging Method

Tishun Peng<sup>1</sup>, Abhinav Saxena<sup>2</sup>, Kai Goebel<sup>3</sup>, Shankar Sankararaman<sup>4</sup>, Yibing Xiang<sup>5</sup>, and Yongming Liu<sup>6</sup>

<sup>1,5,6</sup>*School for Engineering of Matter, Transport and Energy, Arizona State University, Tempe, AZ, 85281, USA*

*tpeng7@asu.edu*  
*yibing.xiang@asu.edu*  
*yongming.liu@asu.edu*

<sup>2,4</sup>*SGT, NASA Ames Research Center, Moffett Field, CA, 94035, USA*

*abhinav.saxena@nasa.gov*  
*shankar.sankararaman@nasa.gov*

<sup>3</sup>*NASA Ames Research Center, Moffett Field, CA, 94035, USA*

*kai.goebel@nasa.gov*

## ABSTRACT

In this paper, a framework for probabilistic delamination location and size detection is proposed. A delamination probability image using Lamb wave-based damage detection is constructed using the Bayesian updating technique. First, the algorithm for the probabilistic delamination detection framework using Bayesian updating (Bayesian Imaging Method - BIM) is presented. Following this, a fatigue testing setup for carbon-carbon composite coupons is introduced and the corresponding lamb wave based diagnostic signal is collected and interpreted. Next, the obtained signal features are incorporated in the Bayesian Imaging Method to detect delamination size and location, as along with corresponding uncertainty bounds. The damage detection results using the proposed methodology are compared with X-ray images for verification and validation. Finally, some conclusions and future works are drawn based on the proposed study.

## 1. INTRODUCTION

Composite materials are widely used in many applications, such as rotorcraft, aerospace, automobiles, and civil engineering structures because of their low weight and high strength properties. Delamination damage may happen within the composite plate due to impact loading or cyclic loadings. Because of the embedded nature of delamination damage, visual inspection is not able to easily detect it and, therefore, nondestructive evaluation (NDE) techniques are

generally used and extensively investigated for this type of diagnosis problems in composites.

Currently, there are many deterministic non-destructive techniques (NDT) available for the delamination diagnosis, such as thermography (Koruk and Kilic 2009; Mielozyk, Krawczuk, Malinowski, Wandowski and Ostachowicz 2012), ultrasonic (Kazys and Svilainis 1997), X-ray (Nicolleto and Hola 2010), and eddy currents (Grimberg, Premel, Savin, Le Bihan and Placko 2001; Sophian, Tian, Taylor and Rudlin 2001). A comprehensive review of these methods for delamination location and size detection is presented in (Cheng and Tian 2012). Most NDE methods require that the specimens to be maintained under certain strict experiment condition for ex-situ damage detection. Alternatively, with the development of Lamb wave-based damage detection methods, piezoelectric sensors have been widely used (Lemistre and Balageas 2001; Giurgiutiu, Zagrai and Bao 2002) for structural health monitoring because of their low cost and high efficiency (Constantin, Sorohan and Gavan 2011). Lamb waves can propagate in thin plate without significant dispersion in certain modes of wave propagation (Scalea, Francesco, Robinson, Tuzzeo and Bonomo 2002). Using proper mode selection, piezoelectric sensor networks can be used for damage inspection of composite plate structures (Wang, Rose and Chang 2004). The advantage of this method lies in that embedded or surface mounted PZTs can be used for in-situ monitoring of structure's health condition. In this technique, damage features are extracted from the received Lamb wave signal using signal-processing algorithms. Several characteristics of the received signal (e.g., the attenuation,

Tishun Peng et al. This is an open-access article distributed under the terms of the Creative Commons Attribution 3.0 United States License, which permits unrestricted use, distribution, and reproduction in any medium, provided the original author and source are credited.

phase shift, energy etc.) indicate changes from baseline i.e. damage features (Raghavan and Cesnik 2007).

For Lamb wave detection methods, there are two common approaches (Raghavan and Cesnik 2007)- (a) pulse-echo, and (b) pitch-catch. Using pulse-echo based approach, damage position can be detected by methods like triangulation, (Su and Ye 2009; Zhou, Su and Cheng 2011) or using cumulative coefficient change (Zhao, Gao, Zhang, Ayhan, Yan, Chiman and Joseph 2007). Furthermore, it also allows estimating detect the damage intensity if damage location is known (Peng, He, Liu, Saxena, Celaya and Goebel 2012). However, most existing damage detection techniques based on Lamb waves are deterministic and cannot systematically include the uncertainties, such as measurement uncertainty and model parameter uncertainty in the damage diagnosis. In view of the above mentioned difficulty, a probabilistic damage detection method for in-situ applications is proposed in this study. This novel method is presented here to simultaneously detect the damage location and size, then provide their confidence information. The proposed method combines the Lamb wave-based damage detection technique and a novel Bayesian Imaging Method (BIM) to achieve this goal.

This paper is organized as follows. First, the Bayesian theorem is introduced and a probabilistic delamination detection, localization, and size estimation framework (Bayesian Imaging Method) is developed. Then, a Lamb wave based test and signal analysis setup is presented for diagnostic feature extraction. Next, an example is presented to validate the proposed Bayesian Imaging method for delamination size and location detection. Damage diagnosis uncertainty bounds are simultaneously generated. Finally, some conclusions and future works are drawn based on the proposed study.

## 2. DAMAGE DIAGNOSIS ALGORITHM USING BAYESIAN IMAGING METHOD

Bayes' theorem is widely used in image processing, which combines the prior distribution of a realistic image and utilizes new measurement data to improve image resolution or segmentation (Li, Dong, Guan, Li and Zhou 2007; Pickup, Capel, Roberts and Zisserman 2009). It is also used to compress the information needed to reconstruct the image by optimizing the basis-function weights, which is a powerful tool to deal with the problem of limited measurements (Ji, Xue and Carin 2008). These methods are explained briefly next.

### 2.1. Bayes' Theorem

Bayes' theorem is commonly used for probabilistic inference or learning process. It can combine the prior belief about parameters and current system response to provide a reasonable prediction of parameters distribution. Let  $p(\theta)$

denote the prior distribution of parameter  $\theta$ . According to the Bayes' theorem, the posterior distribution of  $\theta$  is given as

$$q(\theta) \propto p(\theta)p(x'|\theta) \quad (1)$$

where  $p(x'|\theta)$  is the likelihood function, which reflects the current system response  $x'$  and  $q(\theta)$  is the posterior distribution of updated parameters. Let  $x'$  be an in-situ measurement,  $M(\theta)$  is the prediction value based on a model. If there is no measurement noise or model uncertainty, the measurement would be identical with the model prediction, i.e.  $x' = M(\theta)$ . However, this is usually never the case. Therefore, it is necessary to account for measurement noise  $\epsilon$  and model uncertainties  $\tau$  and the relationship between  $x'$  and  $M(\theta)$  can be expressed as

$$x' = M(\theta) + \epsilon + \tau \quad (2)$$

Assuming that the two error term  $\epsilon$  and  $\tau$  are independent zero mean normal variables (Bell 2001; Adam 2002), the sum of them can be expressed as a new random variable  $e = (\epsilon + \tau) \sim N(0, \sigma_e)$ . Therefore the likelihood function  $p(x'|\theta)$  can be expressed as

$$p(x'_1, x'_2, \dots, x'_n | \theta) = \frac{1}{(\sqrt{2\pi}\sigma_e)^n} \exp\left(-\frac{1}{2}\sum_{i=1}^n \left(\frac{x'_i - M(\theta)}{\sigma_e}\right)^2\right) \quad (3)$$

where  $n$  is the number of available measurements. Substituting Eq. (3) into Eq.(1), the posterior distribution of parameter  $\theta$  is expressed as

$$p(\theta | x'_1, x'_2, \dots, x'_n) \propto p(\theta) \frac{1}{(\sqrt{2\pi}\sigma_e)^n} \exp\left(-\frac{1}{2}\sum_{i=1}^n \left(\frac{x'_i - M(\theta)}{\sigma_e}\right)^2\right) \quad (4)$$

where the posterior distribution of the parameter  $\theta$  can be approximated by the samples drawn by the Markov chain Monte Carlo simulation.

### 2.2. Damage Diagnosis and Bayesian Imaging Development

In the damage detection problem, the sensor signal can be periodically accessed during the servicing operations of structures and signal features can be extracted using appropriate signal processing techniques. To predict the damage size and location, a physics model  $M(\theta)$  describing the relationship between the signal features and damage information should be developed first, which is developed using information extracted from available testing datasets. Next, a likelihood function for the updated parameters, i.e., delamination size and location is built considering the measurement and model uncertainties. Now, the posterior belief about damage can be estimated from the posterior distribution of the updated parameters. In this case the parameter vector  $\theta$  comprises of delamination geometric center coordinate  $(x_0, y_0)$  and delamination size  $a$ . Since no prior belief is available for any of these three parameters,

the prior distribution  $x_0, y_0$  are assumed to be uniform distribution cover the whole possible region where the delamination may appear. The delamination size distribution is uniformly distributed from zero to a large size (e.g, the physical length of the specimen as the largest possible delamination size). A very small quantity (i.e., 0.001 mm) for the delamination distribution lower bound is used to avoid numerical difficulties. The overall diagnosis framework is shown in Fig. 1.

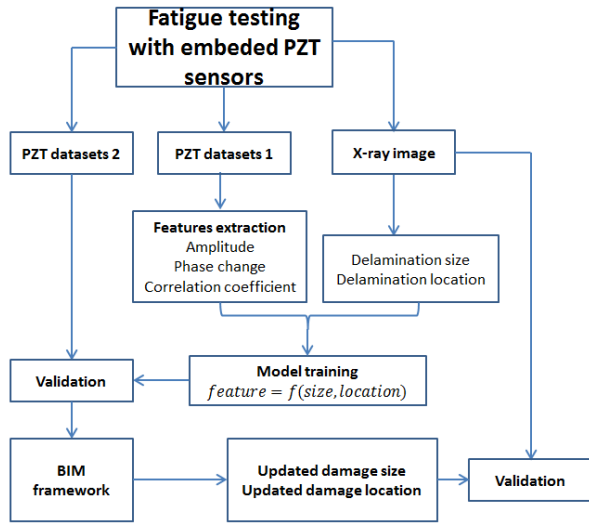


Figure 1. Flowchart for the damage diagnosis method

In Bayesian updating, it is nontrivial to derive an analytical solution if the posterior distribution is non-parametric or very complex, which is the case in this problem. Therefore, the Markov-Chain Monte-Carlo (MCMC) method is used to draw samples. Detailed discussion on MCMC method can be found in several references (Hasting 1970; Peskun 1973; Cowles and Carlin 1996; Fort, Moulines and Priouret 2012) and is, therefore, not discussed here.

The key idea behind the proposed BIM is that the entire specimen is discretized into many small cells (e.g., with size 1mm × 1mm in the current study) and each cell is assigned an associated probability of damage. The probability of damage is updated based on measured signal features using the Bayesian technique. The updated posterior distribution at each cell can be used to construct an image that directly represents the damage location and size.

### 3. DELAMINATION DIAGNOSIS EXPERIMENT USING PIEZOELECTRIC SENSOR

In this section, the proposed BIM is demonstrated using an experimental study. The testing datasets are used to train the model  $M(\theta)$  to get the likelihood function. The Bayesian updating results are compared with X-ray images for model verification and validation. Details are presented next.

### 3.1. Fatigue Cycling Experiment Setup

In a separate effort run-to-failure fatigue experiments were conducted using composite coupons with 12 plies. Torayca T700G uni-directional carbon-prepreg material was used for this 15.24cm × 35.56cm dog bone geometry coupons and a notch (5.08 mm × 19.3mm) is introduced to induce stress concentration, as shown in Fig. 2.

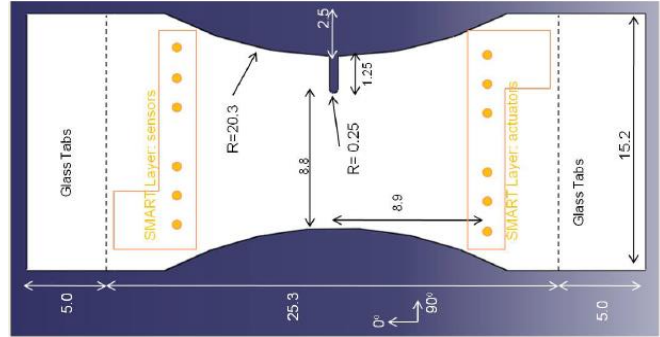


Figure 2. The geometry of the dog bone coupon (unit: cm)

These experiments served several objectives - (i) collection of run-to-failure data with periodic system health data using PZT sensors, (ii) collection of ground-truth data for the delamination to validate the sensor measurement analysis, (iii) accounting for variations between samples of same internal structure (layup), and (iv) characterizing variations between samples of different internal structures. Three symmetric layup configurations were chosen to account for the effect of the ply orientation: Layup 1:  $[0_2/90_4]_2$ , Layup 2:  $[0/90_2/45/-45/90]_2$ , and Layup 3:  $[90_2/45/-45]_2$ . Two six-PZT sensor SMART Layers from Acellent Technologies, Inc (Fig. 3(a)) were attached to the surface of each sample. In Fig. 3(a), actuator 1 to 6 were used to actuate the PZT signal and sensors 7-12 collect the corresponding signal propagation through the plate. Each actuator and sensor acted as a diagnosis path to interrogate the damage information. A more detailed description about these experiments is given in (Saxena, Goebel, Larrosa, Janapati, Roy and Chang 2011). Fig. 3(a) shows such a path form actuator 5 to sensor 8, which is represented as path 5→8. The other paths follow the same rule as above in the following sections.

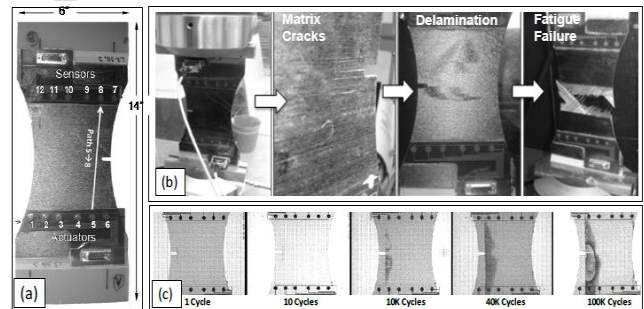


Figure 3. (a) Coupon specimen, SMART layers location, and diagnostic path from actuator 5 to sensor 8, (b) Development of matrix cracks and delamination leading to fatigue failure, (c) Growth in delamination area during the increased loading cycles.

Using this configuration of sensor network, all PZTS are used one by one as actuator to actuate the Lamb wave, which is received by other acting as sensors. It is expected that the growth in delamination size will be captured in the received signals from a particular diagnosis paths that cover delamination area (e.g. path 5→8), which was validated by the comparison between features and delamination size in literature (Saxena, Goebel, Larrosa, Janapati, Roy and Chang 2011). For diagnosis path 5→8, the signal received by sensor 8 at different loading cycles is plotted in Fig. 4. As illustrated in Fig. 4, an increase in delamination size can be captured by monotonic trends in features (amplitude, correlation coefficient, and phase change). Conceptually, a change (decrease) in normalized amplitude reflects the energy dissipation due to the damage. The phase angle change is attributed to the increased wave traveling distance induced by the damage. The correlation coefficient change reflects the signal perturbation due to the new waves generated at the damage surfaces due to reflections (Raghavan and Cesnik 2007). All of these features are computed by comparing the received signal from a pristine coupon, called baseline and the signals from damaged coupons.

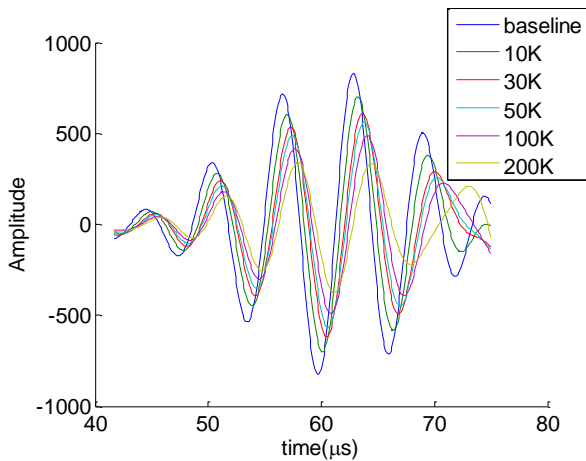


Figure 4. Changes in signal received at sensor 8 as a function increasing fatigue cycles.

### 3.2. Data Processing

Observation from x-ray images of the damaged coupons reveal that damage grows from the tip of the slit in a characteristic way extending as a half elliptical lobes. Therefore, damage shapes are modeled as half elliptical lobes. Using the sensor network and the analysis method described above, there are two parameters describing these

half elliptical shapes that would possibly affect the received signal, which is shown in Fig. 5. The green ellipse is the delamination area observed from the x-rays and the red envelope is introduced to cover the entire area, whose radius is used as a proxy for delamination size  $a$ . The distance from the delamination center to the diagnosis path is denoted by  $d$ . Features extracted from measurements can be related to these two parameters. For instance, corresponding features for actuator 5 are given in Fig. 6.

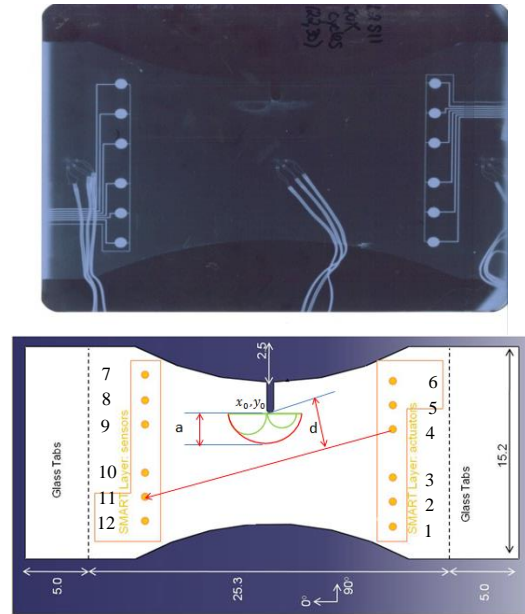
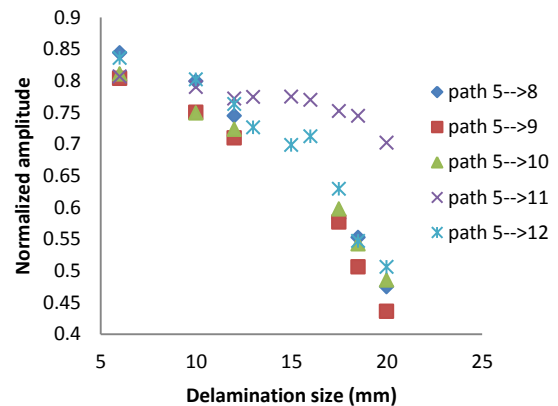


Figure 5. X-ray image and schematic representation delamination



(a)

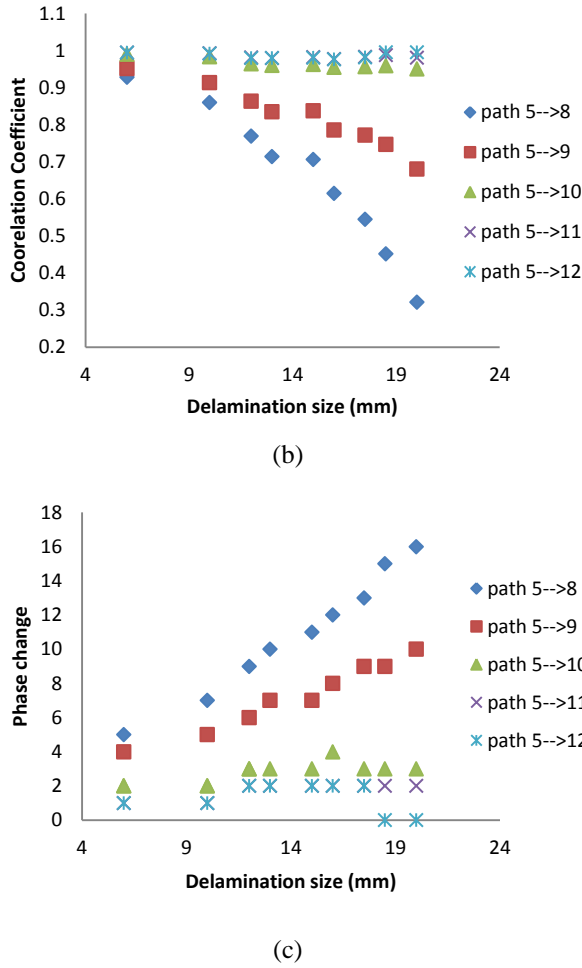


Figure 6. Features related to actuator 5 for different delamination size and distance. (a). Normalized amplitude, (b). Correlation coefficient, (c). Phase change

As shown in Fig. 6, the correlation coefficient and phase change features are more sensitive to the distance compared to the normalized amplitude. For example for a fixed distance, these two features have monotonic relationship with the delamination size, which is consistent with the trend in Fig. 4. In order to use these two features in the BIM proposed earlier, a model is introduced to express the relationship between the features with the delamination size and position. A generic expression can be written as

$$feature = f(a, d) \quad (5)$$

where  $a$  is the delamination size,  $d$  is the distance from the delamination center to the direct diagnosis path. It should be noted that Eq. (5) is a generic expression and does not limit to a specific function type. In this study, a polynomial regression model is used. Using the trend in the datasets, the model used for these two features is given as

$$feature = f_1(d) \times a^2 + f_2(d) \times a + f_3(d) \quad (6)$$

where  $f_i(d) = \beta_{i1} \times \ln(d) + \beta_{i2}$  for correlation coefficient;  $\beta_{ij}$  is regression coefficients, which can be obtained by learning from the training datasets. After tuning these coefficients, the testing and fitted results for features are shown in Fig. 7. The yellow dots are the validation data and the rest are used for the training. It is can be seen that the simple regression model above gives satisfactory results except for the regions where the delamination is far away from the diagnostic path.

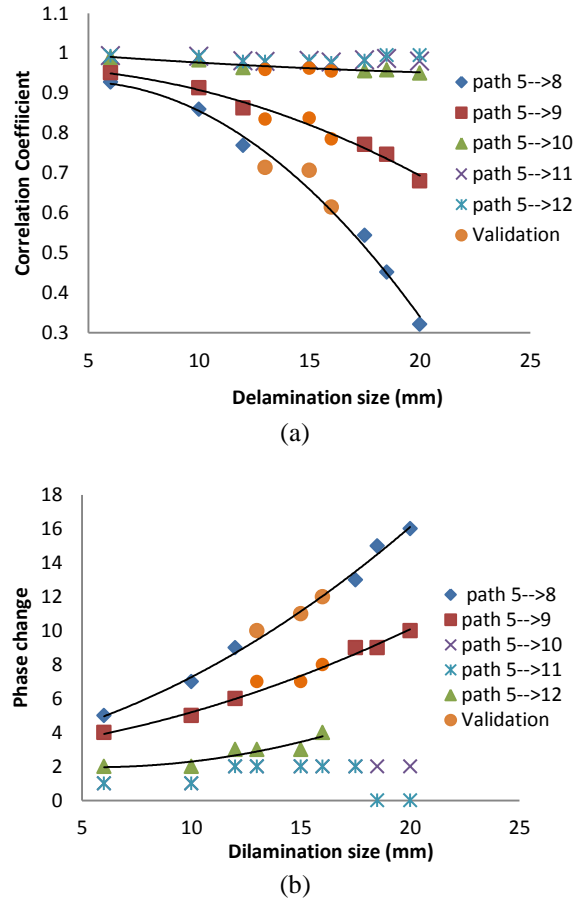


Figure 7. The testing data and curve fitting (a). Correlation coefficient, (b). Phase change

The data analysis presented above is from a single actuator (actuator 5), but a similar trend is observed for data from other actuators. For a given delamination defect, damage information from different actuators and wave paths can be combined to provide a better estimation of the delamination size and location. The following section, presents an example of the BIM method application.

#### 4. DEMONSTRATION EXAMPLE

As described in section 2, the physics model  $M(\theta)$  is needed to show the relationship between damage information and signal features, which can be substituted by the fitting model shown in Eq. (6). The posterior belief about the

damage is estimated by the posterior distribution of the updated parameters. Parameter  $\theta$  represents the delamination center coordinate  $(x_0, y_0)$  and delamination size  $a$ . Since no prior belief is available for these three parameters, the prior distributions of location is assumed to be  $x_0 \sim U(93.5, 259.5)$ ,  $y_0 \sim U(25, 125)$ , which covers all the possible location where delamination may appear. The coordinate definition of this specimen is given in Fig. 8. The delamination size distribution is assumed as  $a \sim U(0.001, 18)$ , where  $U$  means uniform distribution. The likelihood function is built based on the difference between fitting model and real experimental data. The measurements from actuator 5 and 6 are utilized in Bayesian updating, as given in Table 1. It should be noted that each updating iteration incorporates one measurement in the BIM framework. The aspect ratio for these two dimensions are assumed to be 2.5 based on the experimental X-ray image.

Table 1. The sensor measurements for given delamination

Sensor	5		6	
	Correlation Coefficient	Phase change	Correlation Coefficient	Phase change
8	0.7142	10	0.6858	10
9	0.8351	7	0.8279	7
10	0.9595	3	0.9476	4

The posterior distribution of  $(x_0, y_0, a)$  can be estimated by the samples drawn using the MCMC, which updates the belief about the delamination location and delamination size at each updating iteration. At the same time, corresponding median and uncertainty bound predictions are computed to describe the accuracy of each updating result. The delamination location estimates after each updating iteration are shown in Fig. 9.

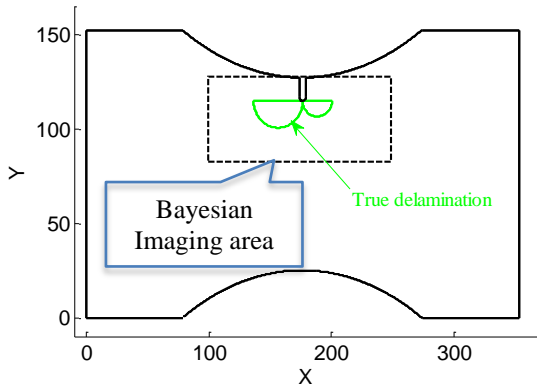


Figure 8. The definition of the sample coordination and specific area to show the Bayesian image

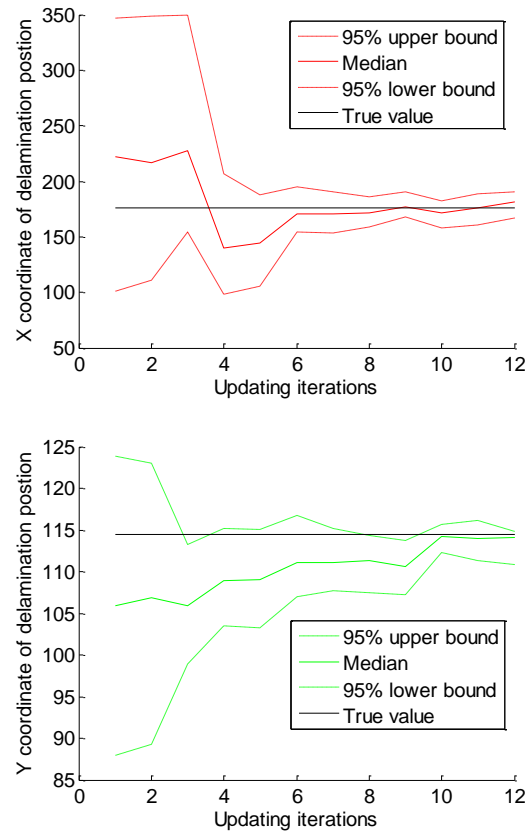
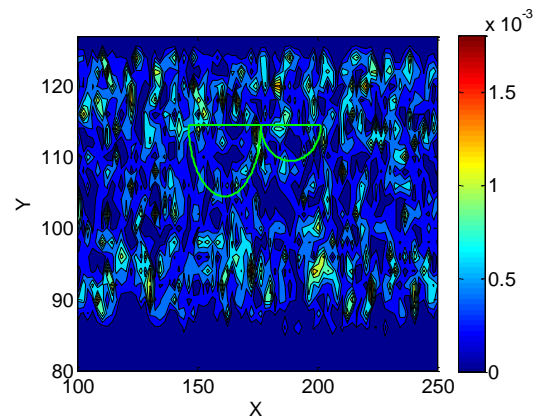


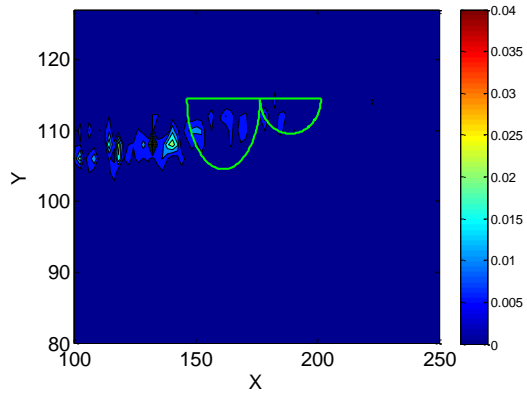
Figure 9. The delamination location updating

As shown here, the estimated delamination location is approaching the true location as more data are used for the updating. Additionally, the uncertainty bounds narrow down as more measurements become available. Fig. 10 illustrates the Bayesian Imaging of the damage probability at each cell of the specimen. It is obvious that the possible delamination area is narrowed down and the probability is increasing as applied more updating iterations. At last, the location with the highest probability is considered as the most probable delamination centers, which is almost the same with the true value as show in Fig. 10(d).

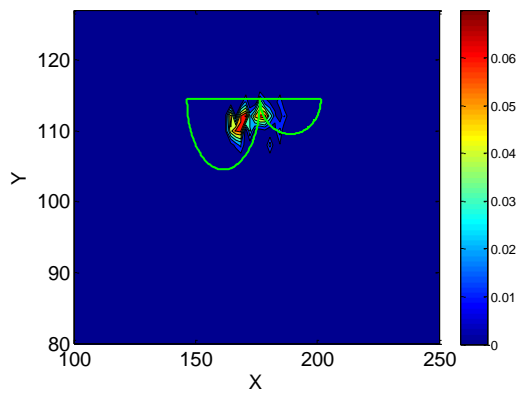


(a) One updating iteration

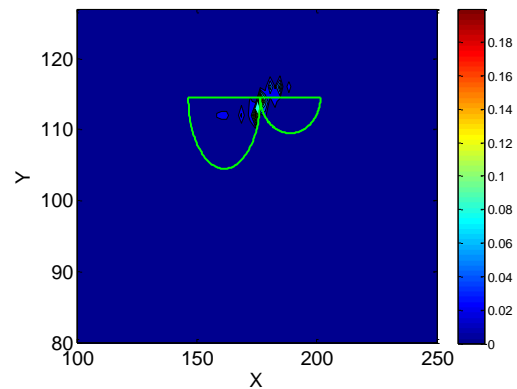




(b) Four updating iterations



(c) Eight updating iterations



(d) Twelve updating iterations

Figure 10. The damage location probability updating at each cell of the plate.

Simultaneously, delamination size is updated gradually, as shown in Fig. 11. By incorporating the location and size information, the estimated delamination area can be calculated. Fig. 12 gives the comparison between the true delamination from the X-ray images and the updated results using the proposed BIM. Satisfactory agreement is observed.

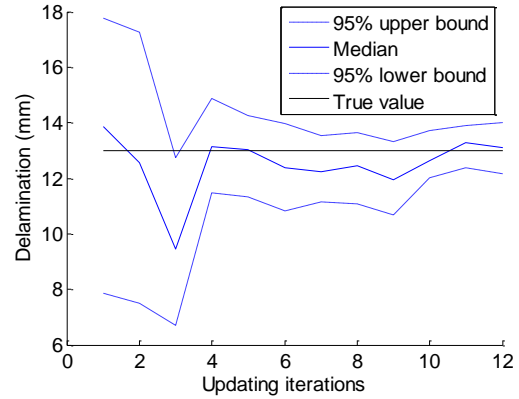
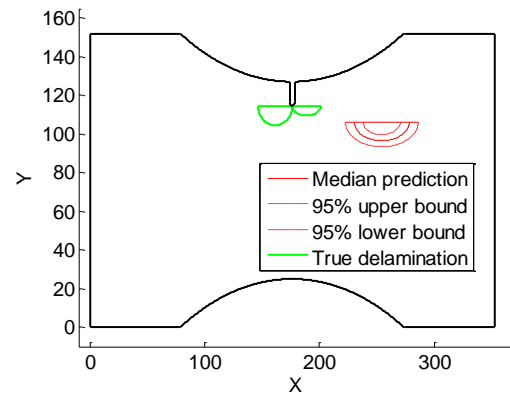
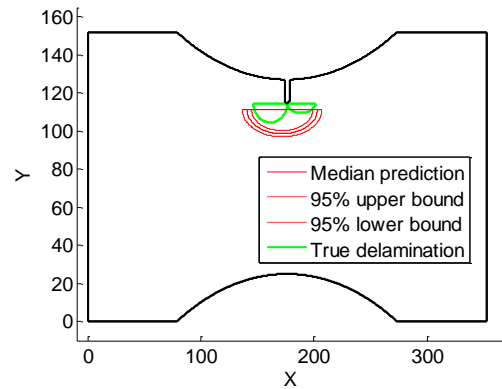


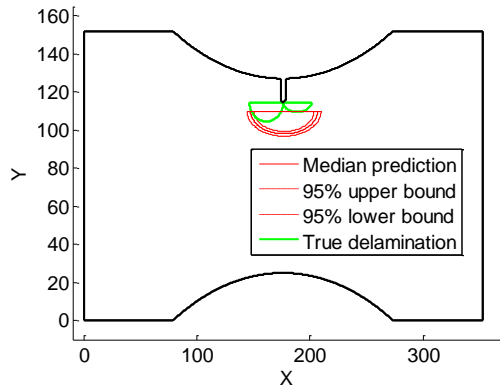
Figure 11. The delamination size updating



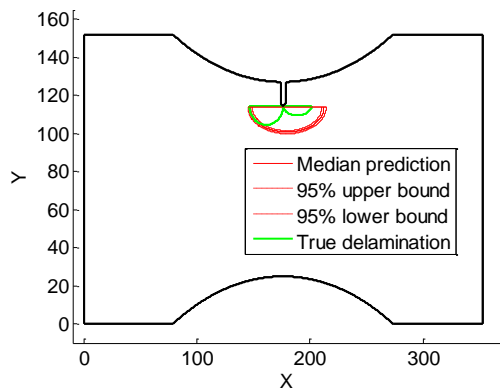
(a) One updating iteration



(b) Four updating iterations



(c) Eight updating iterations



(d) Twelve updating iterations

Figure 12. The comparison between the true value and updating result

As given in Fig. 12, the predicted delamination is reconstructed based on the location and size prediction after each updating iteration. More updating iterations means more information is incorporated in the Bayesian updating. At the same time, the uncertainty bound is decreased as applied more updating iterations, which is consistent with the result given in Fig. 9 and Fig. 11.

## 5. CONCLUSION

In this paper, a probabilistic damage size and location updating algorithm is proposed, which incorporates the Lamb wave based signal features into the Bayesian updating framework. The proposed method is validated by experimental measurements from X-ray images. Based on the results obtained above, several conclusions are drawn:

1. The Lamb wave propagation based SHM method is able to capture the delamination size and location information
2. The correlation coefficient and the phase change in the received signal are more sensitive to the damage location, but they are not very sensitive when the damage is far away from the sensor path.

3. Bayesian updating can represent and manage the damage detection uncertainties, including both modeling uncertainty and measurement uncertainty. Probabilistic estimation of damage size and location can be obtained and the Bayesian image is constructed based on the probability of each cell.

Currently, only two feature are utilized in the Bayesian updating. Further efforts are required to incorporate more features to give a better detection performance. Simultaneous, More parameters need to be found to characterize the delamination besides size and location. Other possible regression models needs further investigation to cancel the uncertainties between different specimens. Additionally, an irregular delamination shape needs further investigation, which can be done by attaching more sensors on the target region.

## ACKNOWLEDGEMENT

The research reported in this paper was partially supported by the NASA through Global Engineering and Materials, Inc. (GEM) under the project NNX12CA86C. The support is gratefully acknowledged.

## NOMENCLATURE

$a$	delamination size
$x'$	Measurement
$x_0$	x coordinate of the delamination center
$y_0$	y coordinate of the delamination center
$\beta_{ij}$	Regression coefficients
$\epsilon$	Measurement noise
$\theta$	Updating parameters
$\tau$	Model uncertainty

## REFERENCES

- Adam, M. T. (2002). "G104-A2L Guide for estimation of measurement uncertainty in testing." American Association of Laboratory Accreditation Manual: 10-18.
- Bell, S. (2001). "A Beginner's Guide to Uncertainty of Measurement." The National Physical Laboratory 2: 9-16.
- Cheng, L. and Tian, G. Y. (2012). "Comparison of Nondestructive Testing Methods on Detection of Delaminations in Composites." *Journal of Sensors* 2012(2012): 7.
- Constantin, N., Sorojan, S. and Gavan, M. (2011). "Efficient and low cost PZT network for detection and localization of damage in low curvature panels." *Journal of Theoretical and Applied Mechanics* 49(3): 685-704.
- Cowles, M. K. and Carlin, B. P. (1996). "Markov Chain Monte Carlo Convergence Diagnostics: A Comparative



- Review." *Journal of the American Statistical Association* 91(434).
- Fort, G., Moulines, E. and Priouret, P. (2012). "Convergence of adaptive and interacting Markov chain Monte Carlo algorithms." *Annals of Statistics* 39(6): 3262-3289.
- Giurgiutiu, V., Zagari, A. and Bao, J. J. (2002). "Piezoelectric wafer embedded active sensors for aging aircraft structural health monitoring." *Structural Health Monitoring* 1(1): 41-61.
- Grimberg, R., Premel, D., Savin, A., Le Bihan, Y. and Placko, D. (2001). "Eddy current holography evaluation of delamination in carbon-epoxy composites." *Insight* 43(4): 260-264.
- Hasting, W. K. (1970). "Monte Carlo sampling methods using Markov Chain and their applications." *Biometrika* 57: 97-109.
- Ji, S., Xue, Y. and Carin, L. (2008). "Bayesian Compressive Sensing." *IEEE transaction on signal processing* 56(6).
- Kazys, R. and Svilainis, L. (1997). "Ultrasonic detection and characterization of delaminations in thin composite plates using signal processing technique." *Ultrasonics* 35: 367-383.
- Koruk, M. and Kilic, M. (2009). "The usage of IR thermography for the temprature measurements inside an automobile cabin." *International Communication in Heat and Mass Tansfer* 36: 872-877.
- Lemistre, M. and Balageas, D. (2001). "Structural health monitoring system based on diffracted Lamb wave analysis by multiresolution processing." *Smart materials and structures* 10: 504.
- Li, Y.-l., Dong, L.-y., Guan, W.-z., Li, Z. and Zhou, L.-y. (2007). "The Application of Bayesian Method in Image Segmentation." *ICICIC '07 Proceedings of the Second International Conference on Innovative Computing, Informatio and Control* 490.
- Mielozyk, M., Krawczuk, M., Malinowski, P., Wandowski, T. and Ostachowicz, W. (2012). "Active therography method for delamination detection and localisation in composite structures." *6th European Workshop on Structural Health Monitoring*
- Nicolleto, A. and Hola, K. (2010). "X-ray computed tomography vs. metallography for pore sizing and fatigue of cast Al-alloys." *Pocedia Engineering* 2(1): 8.
- Peng, T., He, J., Liu, Y., Saxena, A., Celaya, J. and Goebel, K. (2012). "Integrated fatigue damage diagnosis and prognosis under uncertainties." *Annual Conference of Prognostics and Health Management Society*.
- Peskun, P. H. (1973). "Aptimum Monte Carlo sampling using Markov chains." *Biometrika* 57: 97-109.
- Pickup, L. C., Capel, D. P., Roberts, S. J. and Zisserman, A. (2009). "Bayesian Methods for Image Super-Resolution." *THE computer Journal* 52(1): 101-113.
- Raghavan, A. and Cesnik, C. E. S. (2007). "Review of guided-wave structural health monitoring." *Shock and Vibration Digest* 39(2): 91-116.
- Saxena, A., Goebel, K., Larrosa, C. C., Janapati, V., Roy, S. and Chang, F.-K. (2011). "Accelerated Aging Experiments for Prognostics of Damage Growth in Composite Materials." *Proceedings of the 8th International Workshop on Structural Health Monitoring* 1: 1139-1149.
- Scalea, d., Francesco, L., Robinson, J. S., Tuzzeo, D. and Bonomo, M. (2002). "Guided wave ultrasonics for NDE of aging aircraft components " *Proc. SPIE* 4704: 123-132.
- Sophian, A., Tian, G. Y., Taylor, D. and Rudlin, J. (2001). "Electromag-netic and eddy current NDT: a review." *Insight* 43(5): 302-306.
- Su, Z. and Ye, L. (2009). "Identification of damage using Lamb waves: From fundamentals to applications." London: Springer-Verlag GmbH & Co.: 346.
- Wang, C. H., Rose, J. T. and Chang, F.-K. (2004). "A synthetic time-reversal imaging method for structural health monitoring." *J. of smart mater. Struct.* 13: 413-423.
- Zhao, X., Gao, H., zhang, G. f., Ayhan, B., Yan, F., Chiman, K. and Joseph, L. R. (2007). "Active health monitoring of an aircraft wing with embedded piezoelctric sensor/actuator network:I.Defect detection, localization and growth monitoring " *Smart MATER. STRUCT.* 16: 1208-1217.
- Zhou, C., Su, Z. and Cheng, L. (2011). "Probability-based diagnostic imaging using hybrid features extracted from ultrasonic Lamb wave signals." *Smart materials and structures* 20(12): 125005.